Constraints on modified gravity from Sunyaev-Zeldovich cluster surveys

Daisy S. Y. Mak, Elena Pierpaoli, Fabian Schmidt, and Nicolo' Macellari

Phys. Rev. D **85**, 123513 — Published 7 June 2012

DOI: 10.1103/PhysRevD.85.123513

Constraints on Modified Gravity from Sunyaev–Zeldovich Cluster Surveys

Daisy S. Y. Mak,[1,*] Elena Pierpaoli,[1,†] Fabian Schmidt,[2,‡] and Nicolo' Macellari[1,†]

[1] *Physics and Astronomy Department, University of Southern California, Los Angeles, California 90089-0484, USA*
[2] *Theoretical Astrophysics, California Institute of Technology, Pasadena, CA 91125, USA*

We investigate the constraining power of current and future Sunyaev-Zeldovich cluster surveys on the $f(R)$ gravity model. We use a Fisher matrix approach, adopt self-calibration for the mass-observable scaling relation, and evaluate constraints for the SPT, Planck, SPTPol and ACTPol surveys. The modified gravity effects on the mass function, halo bias, matter power spectrum, and mass-observable relation are taken into account. We show that, relying on number counts only, the Planck cluster catalog is expected to reduce current upper limits by about a factor of four, to $\sigma_{f_{R0}} = 2 \times 10^{-5}$ (68% confidence level) while SPT, SPTPol and ACTPol yield about 3×10^{-5}. Adding the cluster power spectrum further improves the constraints to $\sigma_{f_{R0}} = 5 \times 10^{-6}$ for Planck and $\sigma_{f_{R0}} = 2 \times 10^{-5}$ for SPTPol, pushing cluster constraints significantly beyond the limit where number counts have no constraining power due to the chameleon screening mechanism. Further, the combination of both observables breaks degeneracies, especially with the expansion history (effective dark energy density and equation of state). The constraints are only mildly worsened by the use of self-calibration but depend on the mass threshold and redshift coverage of the cluster samples.

PACS numbers: 98.80.-k, 04.50.Kd, 95.36.+x

I. INTRODUCTION

One of the most fascinating aspects of contemporary cosmology is the potential of constraining fundamental physics with the plethora of available data. Galaxy clusters constitute one of the major tools we can use to this aim. The biggest gravitationally bound objects in the Universe, they have formed fairly recently and several of their global properties such as abundance and clustering on large scales can be predicted accurately with theoretical models (e.g., [1, 2]). For this reason, they have been extensively used in the past in order to constrain fundamental parameters such as the total matter density and the matter power spectrum normalization [3–7]. When combined with other cosmological data at various redshifts, clusters can also be used to constrain particle physics and neutrino properties [8–10].

Given that gravity is the only relevant force in the formation of structure in the Universe on large scales, cosmological observations are uniquely suited to test gravity on scales of Mpc, complementing Solar System tests on AU scales. In recent years, clusters have received considerable interest as a probe of gravity [11, 12]. Modifications to gravity generically change the growth of large-scale structure (e.g., [13, 14]), and clusters at the high-mass tail of the mass function are especially sensitive to changes in the growth rate. This has been exploited in Schmidt et al. [15] who used a sample of X-ray clusters to constrain $f(R)$ gravity. Similarly, Lombriser et al. [16] used an optical Sloan cluster sample. A consistency test of the General Relativity + smooth Dark Energy framework using clusters was done in [17].

Here, we focus on the $f(R)$ model of gravity (see [18] for a review), using the functional form proposed in [19]. This functional form satisfies the stability constraint, $d^2 f/dR^2 > 0$, and produces acceleration without a true cosmological constant. In the parameter range of interest here, it is indistinguishable from ΛCDM through geometric probes (CMB, Supernovae, H_0, BAO measurements). However, gravitational forces are modified on smaller scales. Furthermore, the model includes the chameleon screening mechanism which restores General Relativity in high-density environments. Thus, this model is able to satisfy all current constraints on gravity. Structure formation in this modified gravity model is now understood on all cosmological scales: the linear regime of structure formation in this $f(R)$ model has been studied in [19]. The non-linear structure formation was investigated using dedicated N-body simulations in [20–23]. This allows for fully self-consistent constraints and forecasts to be made for this model.

While cluster samples have mainly been selected in the optical and X–ray bands in the past, recent observations based on the Sunyaev–Zeldovich (SZ) effect are starting to produce new detections [24–28]. The SZ effect consists in CMB photons inverse–Compton scattering off electrons in the intra–cluster medium. This process causes a distortion in the CMB blackbody spectrum, and a frequency-dependent brightness change [29]. What makes SZ clusters particularly interesting as cosmological probes is the unique, almost redshift-independent sensitivity for detecting clusters. As a consequence, SZ surveys have the potential to discover clusters at high redshift where optical and X-ray surveys are not very efficient. This new probe is receiving significant attention because of additional data expected from ongoing SZ surveys like Planck, the Atacama Cosmology Telescope (ACT), and the South Pole Telescope (SPT) in the near

*Electronic address: suetyinm@usc.edu
†Electronic address: pierpaol@usc.edu
‡Electronic address: fabians@caltech.edu

future.

In this paper, we explore to what extent these new cluster surveys are expected to constrain $f(R)$ models through cluster number counts and clustering. Cluster surveys are sensitive to both the geometry (expansion history) of the Universe and the growth of structure. The geometry affects the volume covered by a given solid angle and redshift interval, while the growth affects the number density of clusters at a given mass within this volume. For the range of $f(R)$ models considered in this work, chosen to be compatible with solar system constraints, the change in volume is negligible while the one in abundance and clustering of clusters is significant.

The paper is organized as follows. We begin by presenting the surveys and expected cluster samples in Sec. II. This is useful as the modified gravity effects discussed throughout the paper depend sensitively on the characteristics of the cluster samples. In Sec. III we present the parametrization of modified gravity effects on the halo abundance and clustering. Sec. IV details the Fisher formalism employed here, as well as the fiducial cosmology adopted. The forecasted constraints are presented in Sec. V. We discuss our results in Sec. VI and conclude in Sec. VII.

II. CLUSTER SURVEYS

We will investigate the predictions for the four surveys described in the following. While we try to obtain as realistic survey specifications as possible, in particular for the mass limit as function of redshift $M_{\rm lim}(z)$, the lack of previous large samples of SZ clusters necessarily makes these quantities somewhat uncertain. In particular, the relation between cluster mass and SZ signal is still imperfectly known (e.g. [30–33]). The final mass limits as a function of redshift are shown in Fig. 1, and the resulting expected number of clusters for each survey is shown in Fig. 2.

A. The Planck Catalog

Planck is imaging the whole sky with an unprecedented combination of sensitivity ($\Delta T/T \sim 2\times10^{-6}$ per beam at 100 - 217 GHz), angular resolution ($5'$ at 217 GHz), and frequency coverage ($30-857$ GHz). The SZ signal is expected to be detected from a few thousand individual galaxy clusters. Planck will produce a cluster sample with median redshift ~ 0.3 (see Fig. 2, upper left panel). The SZ observable is the integrated Comptonization parameter $Y = \int y\, d\Omega_{\rm cluster}$ out to a given radius. For Planck, a 5σ detection threshold ensuring high level of completeness (about 90%) corresponds to $Y_{200,\rho_c} \geq 2\times10^{-3}{\rm arcmin}^2$ [34], where Y_{200,ρ_c} is the integrated comptonization parameter within r_{200,ρ_c}, the radius enclosing a mean density of 200 times the critical density. The early release from the Planck Collaboration gives a sample of 189 high signal-to-noise SZ clusters with $\geq 6\sigma$ detection. It is therefore likely that our assumed detection threshold will be eventually reached in future data releases. For an SZ survey, its flux limit can be translated into a limiting mass by using simulation-calibrated scaling relations [35]:

$$\frac{M_{\rm lim,200\rho_c}(z)}{10^{15}M_\odot} = \left[\left(\frac{D_A(z)}{{\rm Mpc}/h_{70}}\right)^2 E(z)^{-2/3}\frac{Y_{200,\rho_c}}{2.5\times10^{-4}}\right]^{0.533}. \quad (1)$$

In order to mitigate the effect of overestimation of unresolved clusters at low redshift, we further restrict $M_{\rm lim,200\rho_c}$ to be at least $10^{14}M_\odot$ at all z. With all these criteria, the Planck survey is expected to detect ~ 1000 clusters. The mass threshold we find with this approach is consistent with the one in [36]. While we keep $Y_{200,\rho_c} = 2\times10^{-3}{\rm arcmin}^2$ as our reference minimum value for presentation of the main results, we will also discuss predictions for a lower mass threshold, corresponding to $Y_{200,\rho_c} = 10^{-3}{\rm arcmin}^2$. With such threshold, the completeness of the $S/N > 5$ sample is reduced to about 70% and the total number of clusters is 2700.

B. SPT and SPTpol

The SPT survey is currently observing the sky with a sensitivity of $18\mu{\rm K/arcmin}^2$ at 148 GHz, 218 GHz, and 277 GHz. This survey covers $\Omega \approx 2500$ square degrees of the southern sky (between $20h \geq {\rm RA} \geq 7h$, $-65^\circ \leq \delta \leq -30^\circ$) with a projected survey size and cluster mass limit well matched to the Stage III survey specification of the Dark Energy Task Force [37]. For the mass limits, we employ the calibrated selection function of the survey by [37]. This is based on simulations and used to provide a realistic measure of the SPT detection significance and mass. Disregarding the scatter in the fitting parameters for this relation, we use here:

$$\frac{M_{\rm lim,200\bar{\rho}}(z)}{5\times10^{14}M_\odot h^{-1}} = \left[\left(\frac{\sqrt{\xi^2-3}}{6.01}\right)\left(\frac{1+z}{1.6}\right)^{-1.6}\right]^{1/1.31} \quad (2)$$

where ξ is the detection significance. For the SPT survey, we take clusters detected at $\xi > 5$ which ensure a 90% purity level. Currently, the SPT team is setting a low redshift cut at $z_{\rm cut} = 0.3$ in their released cluster sample, due to difficulties in reliably distinguishing low-redshift clusters from CMB fluctuations in single frequency observations. Nevertheless, with upcoming multi-frequency observations, a lower cut $z_{\rm cut} = 0.15$ will likely be attained. We therefore apply this cut in our work. With this, the SPT survey is expected to detect ~ 500 clusters.

In addition to this, we also consider the upcoming SPT polarization survey (hereafter SPTpol) which will have an increased sensitivity of $4.5\mu{\rm K/arcmin}^2$ at 150 GHz for a 3 year survey and sky coverage of 625 square degrees. We scaled the mass limits by a factor of 3.01/5.95

in Eq. (2) to match with the expected mass limits of SPTpol clusters (Benson 2011, private communication). We again use $z_{\rm cut} = 0.15$, resulting in a total expected number of ~ 1000 clusters. While these are the limits we use for our main results, we also discuss outcomes that consider a lower mass limit, corresponding to $\xi = 4.5$ (80% purity). With this mass limit, SPT would find 800 clusters and SPTPol about 1400 clusters.

C. ACTpol

The Atacama Cosmology Telescope (ACT) has been observing a portion of the southern sky since 2008 consisting of two strips of the sky, each 4 degrees wide in declination and 360 degrees around in right ascension, one strip is centered at $\delta = -5^\circ$, and the other is centered at $\delta = -55^\circ$ [35]. With a sensitivity of $\approx 35\mu$K/arcmin^2, only about 100 clusters are expected to be detected. Instead, we turn to the newly developing dual-frequency (150 GHz and 220 GHz) polarization sensitive receiver (hereafter ACTpol [38] and reference therein) to be deployed on ACT in 2013. One of the three ACTpol observing seasons will have a wide survey covering 4000deg^2 to a target sensitivity of 20μK/arcmin^2 in temperature at 150 GHz. With the wide field, they aim to find ~ 600 clusters in the ACTpol survey. The survey is 90% complete above a limiting mass of $M_{\rm lim,200\bar{\rho}} = 5 \times 10^{14} M_\odot h^{-1}$ (Sehgal 2011, private communication), and we therefore assume this as our redshift-independent mass limit for ACTpol. As in SPT, the ACT team also put a low redshift cut in their parameter determination works and we likewise take $z_{\rm cut} = 0.15$ for ACTpol, resulting in a total expected number of ~ 500 clusters. We also present in the discussion section the results corresponding to a lower mass limit, $M_{\rm lim,200\bar{\rho}} = 4 \times 10^{14} M_\odot h^{-1}$, which would result in a catalog of about 1000 clusters.

III. THEORETICAL MODELING

A. $f(R)$ gravity

In the $f(R)$ model (see [18, 39] and references therein), the Einstein-Hilbert action is augmented with a general function of the scalar curvature R [40–42],

$$S_G = \int d^4x\sqrt{-g}\left[\frac{R + f(R)}{16\pi G}\right]. \tag{3}$$

Here and throughout $c = \hbar = 1$. This theory is equivalent to a scalar-tensor theory (if the function f is nontrivial). The additional field given by $f_R \equiv df/dR$ mediates an attractive force whose physical range is given by the Compton wavelength $\lambda_C = a^{-1}(3df_R/dR)^{1/2}$. On scales smaller than λ_C, gravitational forces are increased by 4/3, enhancing the growth of structure.

A further important property of such models is the non-linear chameleon effect which shuts down the enhanced forces in regions with deep gravitational potential wells compared with the background field value, $|\Psi| > |f_R(\bar{R})|$ [19, 43]. This mechanism is necessary in order to pass Solar System tests which rule out the presence of a scalar field locally. Thus, Solar System tests constrain the amplitude of the background field to be less than typical cosmological potential wells today ($\sim 10^{-5}$).

In this paper, we will choose the functional form introduced by Hu & Sawicki [19]:

$$f(R) = -2\Lambda\frac{R}{R + \mu^2}, \tag{4}$$

with two free parameters, Λ, μ^2. Note that as $R \to 0$, $f(R) \to 0$, and hence this model does not contain a cosmological constant. Nevertheless, as $R \gg \mu^2$, the function $f(R)$ can be approximated as

$$f(R) = -2\Lambda - f_{R0}\frac{\bar{R}_0}{R}\,, \tag{5}$$

with $f_{R0} = -2\Lambda\mu^2/\bar{R}_0^2$ replacing μ as the second parameter of the model. Here we define $\bar{R}_0 = \bar{R}(z = 0)$, so that $f_{R0} = f_R(\bar{R}_0)$, where overbars denote the quantities of the background spacetime. Note that $f_{R0} < 0$ implies $f_R < 0$ always, as required for stable cosmological evolution. If $|f_{R0}| \ll 1$, the curvature scales set by $\Lambda = \mathcal{O}(R_0)$ and μ^2 differ widely and hence the $R \gg \mu^2$ approximation is valid today and for all times in the past.

The background expansion history thus mimics ΛCDM with Λ as a true cosmological constant to order f_{R0}. Therefore in the limit $|f_{R0}| \ll 10^{-2}$, the $f(R)$ model and ΛCDM are essentially indistinguishable with geometric tests. The linear growth rate is identical to that of ΛCDM on scales larger than λ_C, and becomes strongly scale-dependent on smaller scales [19].

Note that we have chosen a model whose expansion history is close to ΛCDM by construction. In general, there is sufficient freedom in the free function f to emulate any given expansion history [44]. Hence, below we will also allow the expansion history to vary, parametrized by effective dark energy parameters w_0 and w_a. Further, while we choose a specific functional form for $f(R)$ here, it is straightforward to map constraints onto different functional forms (see [45] for details). In the following, for notational simplicity f_{R0} will always refer to the absolute value of the field amplitude today.

B. Cluster abundance in $f(R)$

Studying structure formation in $f(R)$ gravity beyond linear theory is complicated by the non-linear field equation for the scalar field f_R, the non-linearity being responsible for the chameleon mechanism. The field equation needs to be solved simultaneously with the evolution

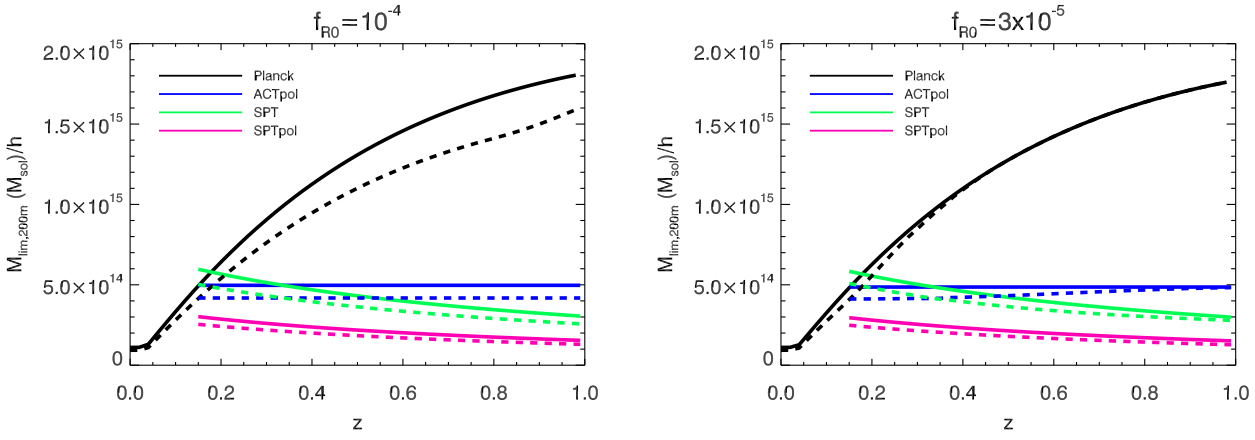

FIG. 1: Mass limit of cluster surveys in ΛCDM (solid) and $f(R)$ gravity (dashed) with $f_{R0} = 10^{-4}$ (left) and $f_{R0} = 3 \times 10^{-5}$ (right). The mass limits in $f(R)$ are reduced due to the effect on dynamical mass measurements (Sec. III A).

of the matter density. This has been done in the self-consistent N-body simulations of [20]. The abundance of dark matter halos (mass function) and their clustering (halo bias) in the $f(R)$ simulations was studied in [22].

Since these simulations are very time-consuming, they cannot be used to exhaust the cosmological parameter space. Instead, we use a simple model developed in [22] based on spherical collapse and the peak-background split in order to predict the cluster abundance and their linear bias.

In order to describe the effect of $f(R)$ gravity on the halo mass function, we employ the Sheth-Tormen prescription for the comoving number density of halos per logarithmic interval in the *virial* mass $M_{\rm v}$, given by

$$n_{\rm v}^{\rm (ST)} \equiv \frac{dn}{d\ln M_{\rm v}} = \frac{\bar{\rho}_{\rm m}}{M_{\rm v}} f(\nu) \frac{d\nu}{d\ln M_{\rm v}}\,, \qquad (6)$$

where the peak threshold $\nu = \delta_c/\sigma(M_{\rm v})$ and

$$\nu f(\nu) = A\sqrt{\frac{2}{\pi}a\nu^2}[1 + (a\nu^2)^{-p}]\exp[-a\nu^2/2]\,. \qquad (7)$$

Here $\sigma(M)$ is the variance of the linear density field convolved with a top hat of radius r that encloses $M = 4\pi r^3\bar{\rho}_{\rm m}/3$ at the background density

$$\sigma^2(r) = \int \frac{d^3k}{(2\pi)^3}|\tilde{W}(kr)|^2 P_L(k)\,, \qquad (8)$$

where $P_L(k)$ is the linear power spectrum (either in ΛCDM or in $f(R)$) and $\tilde{W}$ is the Fourier transform of the top hat window. The normalization constant A is chosen such that $\int d\nu f(\nu) = 1$. The parameter values of $p = 0.3$, $a = 0.75$, and $\delta_c = 1.673$ for the spherical collapse threshold have previously been shown to match simulations of ΛCDM at the $10 - 20\%$ level. The virial mass is defined as the mass enclosed at the virial radius $r_{\rm v}$, at which the average density is $\Delta_{\rm v}$ times the mean density. We transform the virial mass to the desired overdensity criterion $\Delta = 500/\Omega_m$ assuming a Navarro-Frenk-White [46] density profile [47], and assuming the mass-concentration relation of [48] (note that the rescaling depends very weakly on the assumed halo concentration for the values of Δ used here). We thus obtain the mass function of halos in the ST prescription, $n^{\rm (ST)}$, from $n_{\rm v}^{\rm (ST)}$.

The effects of $f(R)$ modified gravity enter in two ways in this prescription: first, we use the linear power spectrum for the $f(R)$ model in Eq. (8). Second, we assume modified spherical collapse parameters which were obtained by rescaling the gravitational constant by 4/3 during the collapse calculation as well as the corresponding linear growth extrapolation to obtain δ_c. This corresponds to the case where the collapsing region is always smaller than the Compton wavelength of the field. Schmidt et al. [22] showed that this case always underestimates the $f(R)$ effects on the mass function and bias, and hence serves as conservative model. For our fiducial cosmology at $z = 0$, we obtain GR collapse parameters of $\delta_c = 1.675$, $\Delta_{\rm v} = 363$, while the modified parameters are given by $\delta_c = 1.693$, $\Delta_{\rm v} = 292$. The Sheth-Tormen prescription itself does not provide a very accurate prediction for the abundance of clusters in ΛCDM in the entire redshift range relevant for SZ surveys. Since more precise parametrizations are available, we only use the ST prescription to predict the relative *enhancement* of the cluster abundance in $f(R)$. Specifically, after rescaling to our adopted mass definition, we take the ratio of the two and multiply it by the ΛCDM mass function from Tinker et al. [1],

$$n(M,z) = n^{\rm (T)}_{\Lambda{\rm CDM}}(M,z)\frac{n^{\rm (ST)}_{f(R)}(M,z)}{n^{\rm (ST)}_{\Lambda{\rm CDM}}(M,z)}, \qquad (9)$$

where we use the parameters given in their Appendix B. Note that for small field values and at high masses,

the predicted $f(R)$ mass function in fact becomes smaller than that for ΛCDM. Since this effect is not seen in the simulations, we conservatively set the mass function ratio to 1 whenever it is predicted to be less than 1.

Fig. 2 shows the number of clusters as a function of redshift expected from the four surveys considered in this work (see Sec. II), and the relative deviations of the $f(R)$ model from the ΛCDM model for different values of f_{R0} (dashed lines). The $f(R)$ modifications are most prominent at low redshifts $z \lesssim 0.4$, since the changes in the linear power spectrum are restricted to progressively smaller scales towards higher redshifts. Further, for $f_{R0} < 5\times10^{-5}$, we see the strongest effects for surveys with the lowest mass thresholds, in particular Planck (for $z < 0.15$) and SPTpol. This is a consequence of the chameleon mechanism which suppresses the mass function enhancement above progressively lower masses as f_{R0} decreases. There are negligible differences between $f(R)$ and ΛCDM for $f_{R0} < 3\times10^{-5}$ at high halo masses. Hence, the mass threshold of a given survey determines what field values can be probed by number counts.

Further, we have to take into account the effect of modified gravity on the mass-observable relation. The SZ effect is a dynamical mass measure, as the decrement Y is proportional to the velocity dispersion (pressure) of electrons. In modified gravity, dynamical mass estimates are generally different from the actual mass due to the presence of the additional gravitational force which enters the virial equation. As shown in [49], the dynamical mass is related to the true mass via

$$M_{\rm dyn} = \overline{g}^{3/5}\, M, \tag{10}$$

where $\overline{g}$ is a weighted integral of the force modification over the object which describes the effect on the virial equation. In principle, $\overline{g}$ should be weighted by the SZ emissivity and observational window function. However in the interest of simplicity, and since we are only interested in an approximate forecast, we simply weight the modified forces by the matter density $\rho_{\rm NFW}(r)$ of the halo, assuming an NFW profile [46]. Further, we assume the host halo is spherically symmetric. We then have

$$\overline{g} = \frac{\int_0^{r_{\rm v}} dr\, r^2\, \rho_{\rm NFW}(r)\, g(r)\, r\, d\Psi_N/dr}{\int_0^{r_{\rm v}} dr\, r^2\, \rho_{\rm NFW}(r)\, r\, d\Psi_N/dr}, \tag{11}$$

where Ψ_N is the Newtonian potential of the halo, found by solving (see [49] for an explicit expression)

$$\nabla^2\Psi_N = 4\pi G\rho_{\rm NFW}, \tag{12}$$

and $g(r)$ is the force modification. In order to calculate the force modification, we have to solve the chameleon field equation for an NFW halo [49]. This calculation is computationally expensive, so we instead use a simple model which describes the exact results reasonably well [49]; in fact it underpredicts the exact result for the force modification, and thus is a conservative estimate. Specifically,

$$g(r) \approx 1 + \frac{1}{3}\frac{M(<r) - M(<r_{\rm scr})}{M(<r)} \tag{13}$$

Here, $r_{\rm scr}$ is the outermost radius at which the condition $|\Psi_N| \geq 3|\bar{f}_R|/2$ is met. In the large-field limit this condition is never met, so that $r_{\rm scr} = 0$ and $g(r) = 4/3$ throughout. Eq. (10) then yields $M_{\rm dyn}/M = (4/3)^{3/5} \approx 1.22$. For sufficiently small fields, the chameleon mechanism becomes active so that $g(r) \to 0$ for $r < r_{\rm scr}$, thus modeling the screening of the modified force. In this case, $M_{\rm dyn}$ will interpolate between M and $1.22M$.

We show in Fig. 1 the mass threshold of the four cluster surveys in ΛCDM (solid) and the $f(R)$ dynamical mass effect to these thresholds (dashed). Fig. 2 also shows the dynamical mass effect on the observed cluster abundance (dash-dotted lines). Note that the dynamical mass effect is not simply additive to the mass function enhancement, since the latter depends on mass as well. Due to the steepness of the halo mass function at the high-mass end, the fact that $M_{\rm SZ} = M_{\rm dyn}$ is larger than the true mass M significantly boosts the abundance of detected clusters above the mass threshold. The two effects of enhanced growth and increased $M_{\rm dyn}$ both contribute to increase the observed cluster abundance. For $z \lesssim 0.4$, the mass function enhancement provides a significant contribution to the overall change in number counts, while at higher redshifts the increase in dynamical mass is the dominant effect.

C. Halo clustering in $f(R)$

In addition to the halo abundance, $f(R)$ modified gravity also affects the clustering of halos. This effect comes from two sources: first, the matter power spectrum is enhanced on small scales by the increased gravitational forces. Second, the linear bias $b_L(M)$ of halos at a given mass M is reduced, since at a fixed mass halos are less rare in $f(R)$ than in GR. The power spectrum of clusters of mass M is modeled as

$$P_h(k, z|M) = [b_L(M, z)]^2 P_L(k, z). \tag{14}$$

For the linear bias $b_L(M)$, we adopt an analogous prescription as for the mass function Eq. (9),

$$b_L(M, z) = b^{\rm (T)}_{L,\Lambda{\rm CDM}}(M, z)\frac{b^{\rm (ST)}_{L,f(R)}(M, z)}{b^{\rm (ST)}_{L,\Lambda{\rm CDM}}(M, z)}, \tag{15}$$

where $b^{\rm (T)}_{L,\Lambda{\rm CDM}}$ denotes the bias fitting formula from Tinker et al. [50], and $b^{\rm (ST)}_L$ is the peak-background split bias derived from the Sheth-Tormen mass function,

$$b_L(M) = 1 + \frac{a\nu^2 - 1}{\delta_c} + \frac{2p}{\delta_c[1 + (a\nu^2)^p]}, \tag{16}$$

where ν, a, p are defined after Eq. (6). Note that ν is given in terms of the virial mass $M_{\rm v}$, and thus for a given mass and redshift ν differs in $f(R)$ due to both the modified spherical collapse parameters and the different linear power spectrum.

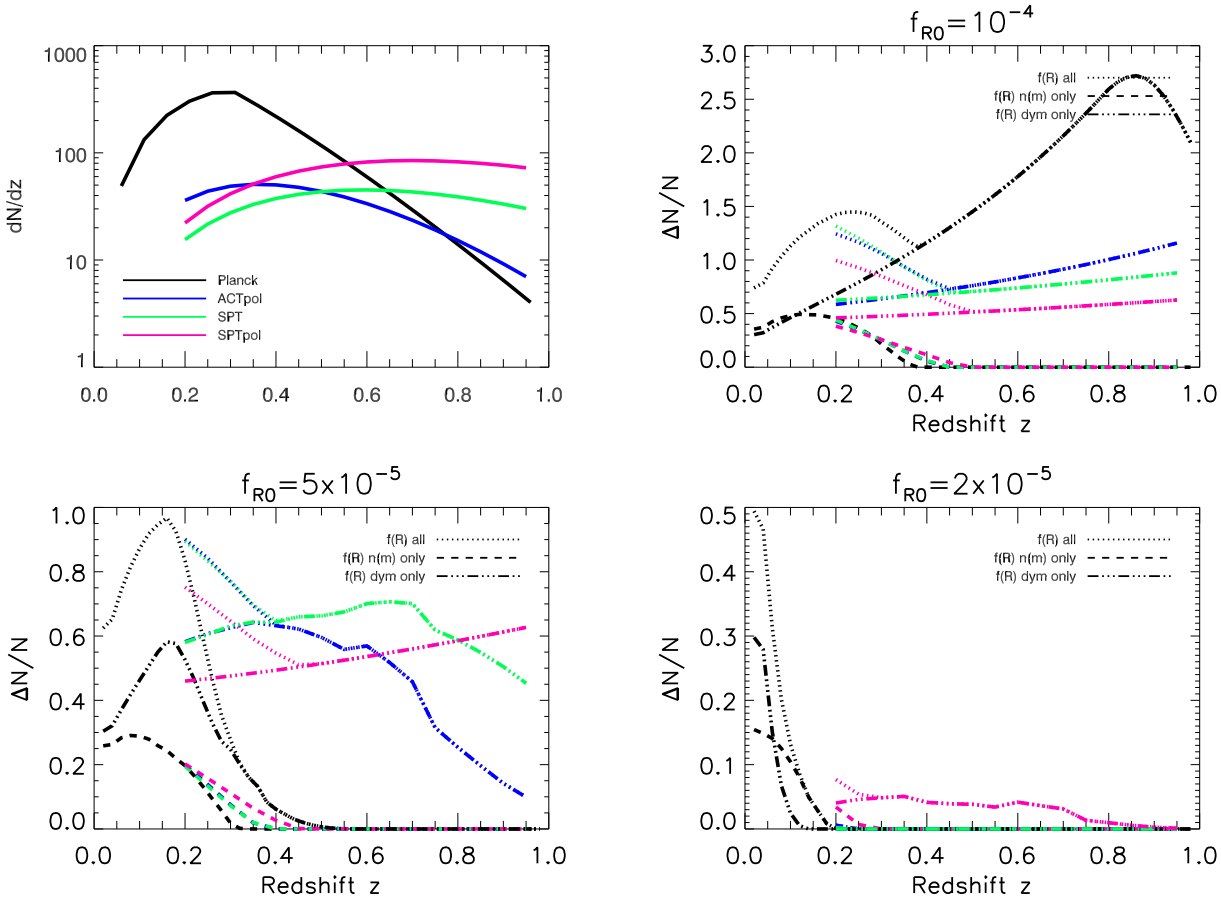

FIG. 2: *Upper left.* The redshift distribution of clusters in the Planck (black), ACTpol (blue), SPT (green), and SPTpol (magenta) survey in the fiducial ΛCDM cosmology. *Upper right, bottom left, bottom right.* The fractional deviation of the number density between $f(R)$ and ΛCDM models due to all effects of $f(R)$ (dotted lines), $\Delta n_{\rm ln}$ effect only (dashed lines), and dynamical mass effect only (dot-dashed lines) evaluated at $f_{R0} = 10^{-4}$, $f_{R0} = 5 \times 10^{-5}$, and $f_{R0} = 2 \times 10^{-5}$ respectively. For the largest field value, the effect on the mass function dominates the enhancement of the cluster abundance at low z, while the dynamical mass effect dominates at $z \gtrsim 0.3$. The Planck and SPTpol survey have the lowest mass threshold at $z < 0.2$ and $z > 0.2$ respectively and hence are most sensitive to the $f(R)$ effects for small field values.

For the matter power spectrum in Eq. (14), we use the linear theory power spectrum for $f(R)$ and ΛCDM. As shown in [21], this describes the non-linear power spectrum at $z = 0$ measured in $f(R)$ N-body simulations up to scales $k \sim 0.2h$/Mpc. In order to minimize the impact of non-linearities on the power spectrum and its covariance, we limit our Fisher matrix to modes with k less than $0.1h$/Mpc. Note that including smaller scales will further improve the constraints; however, a more sophisticated model including non-linear and/or scale-dependent bias, and the non-linear matter power spectrum would be necessary in this case.

Thus, the effect on the cluster power spectrum is due to three combined effects: enhancement of the linear power spectrum $\Delta P_L(k)$, halo bias $\Delta b_L(M, z)$, and the dynamical mass effect $M_{\rm dyn}$. Fig. 3 shows the relative deviation $\Delta P_h/P_h$ of the cluster power spectrum in $f(R)$ with respect to ΛCDM for the Planck survey (Sec. II) as a function of redshift and wavenumber k. Plots for the other surveys investigated here show similar $z-$ and $k-$dependences, though the amplitude of each effect depends on the survey. Here, we have assumed one mass bin $M > M_{\rm lim}(z)$ and $f_{R0} = 10^{-5}$. Similar to dN/dz, we plot the total effect (upper left), and separately the effect due to $\Delta P_L(k)$ (upper right), and $\Delta b_L(M, z)$ (lower panel). For this field value, the dynamical mass effect is irrelevant since the clusters detectable by Planck are chameleon-screened. The departure from ΛCDM is mainly driven by $\Delta b_L(M, z)$ which shows a strong redshift dependence, and only mildly affected by $\Delta P_L(k)$ which is k-dependent and only relevant on small scales. Given that the power spectrum is shot-noise dominated at all scales for the cluster samples considered, the effect on the linear halo bias in fact is the most important contribution to the $f(R)$ constraints from the cluster power spectrum.

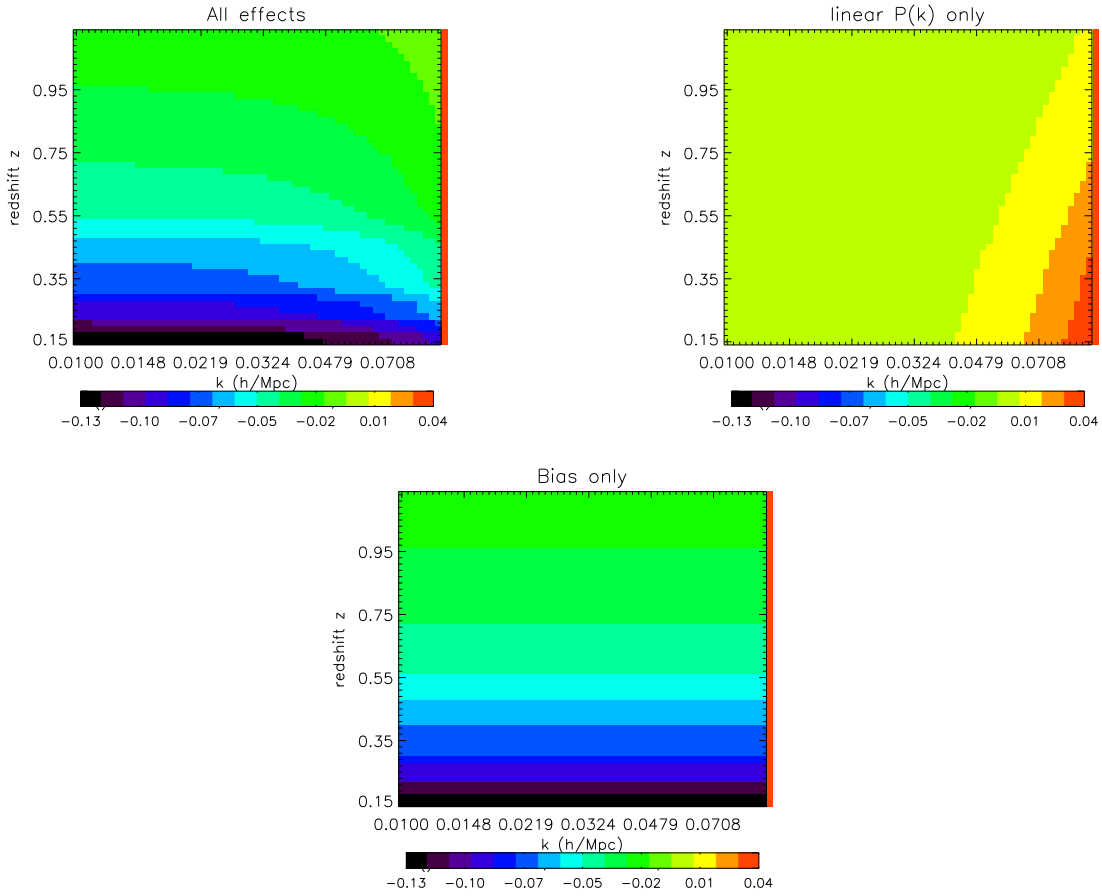

FIG. 3: Relative deviations in the $f(R)$ halo power spectrum from ΛCDM, i.e. $\Delta P_h/P_h$ for the Planck survey, with $|f_{R0}| = 10^{-5}$. *Upper left.* Total deviation. *Upper right.* Deviation due to $P_L(k)$ only. *Lower left.* Deviation due to halo bias b_L only. For this value of f_{R0}, the dynamical mass effect on the power spectrum is negligible and therefore we do not show it here. The redshift and scale dependence in the relative deviations from other cluster surveys are similar to the ones shown here.

IV. FISHER MATRIX FORMALISM

The Fisher information Matrix (FM hereafter) is defined as

$$F_{\alpha\beta} \equiv -\left\langle \frac{\partial^2 \ln \mathfrak{L}}{\partial p_\alpha p_\beta} \right\rangle \tag{17}$$

where $\mathfrak{L}$ is the likelihood of a data set, e.g. a cluster sample, written as a function of the parameters p_α describing the model. The parameters p_α comprise the cosmological model parameters as well as "nuisance" parameters related to the data set (e.g., mass calibration).

A. Cosmological parameters

Throughout this paper, we assume a spatially flat ($\Omega_k = 0$) cosmology. Our model comprises a total of seven cosmological parameters and one $f(R)$ model parameter which are left free to vary. The seven parameters and their fiducial values (in parenthesis, taken from the best-fit flat ΛCDM model from WMAP 7yr data, BAO and H_0 measurements [51]) are: baryon density parameter $\Omega_b h^2(0.0245)$; matter density parameter $\omega_m \equiv \Omega_m h^2$ (0.143); dark energy density $\Omega_\Lambda = 1 - \Omega_m$ (0.73); power spectrum normalization σ_8 (0.809); index of power spectrum n_s (0.963); effective dark energy equation of state through $w(z) = w_0 + (1-a)w_a$, with fiducial values $w_0 = -1$ and $w_a = 0$. The Hubble parameter is then a derived parameter given by $h = \sqrt{\omega_m/(1-\Omega_\Lambda)} = 0.73$ in the fiducial case. The $f(R)$ modification can alternately be parametrized using the field amplitude f_{R0} at $z = 0$, or the Compton wavelength λ_{C0} at $z = 0$ (see Sec. IV F). Our fiducial value is $f_{R0} = \lambda_{C0} = 0$.

In the following, we first discuss the Fisher matrix for number counts and clustering of clusters, before describing the calibration parameters and CMB priors. Throughout, we divide the redshift range into bins l of

width $\Delta z = 0.02$. Further, we bin clusters in logarithmic mass bins m of width $\Delta \ln M = 0.3$ from the minimum mass $M_{\rm lim}(z)$ for each survey (Sec. II) up to a large cut-off mass of $M_{\rm max} = 10^{16} M_\odot$. Since the mass limit varies with redshift, the number of mass bins thus also varies somewhat across the redshift range.

B. Number counts

The FM for the number of clusters $N_{l,m}$ within the l-th redshift bin and m-th mass bin is

$$F_{\alpha\beta} = \sum_{l,m} \frac{\partial N_{l,m}}{p_\alpha} \frac{\partial N_{l,m}}{p_\beta} \frac{1}{N_{l,m}} \tag{18}$$

where the sum over l and m runs over intervals in the whole redshift range $z = 0 - 1$ and cluster mass range $[M_{\rm lim}(z), \infty]$. We can write the abundance of clusters expected in a survey, within a given redshift and mass interval, using the mass function as:

$$N_{l,m} = \Delta\Omega \Delta z \frac{d^2V}{dz d\Omega} \int_{M_{l,m}}^{M_{l,m+1}} dM^{\rm ob} \int_0^\infty d\ln M \; n(M,z) p(M^{\rm ob}|M) \tag{19}$$

where $\Delta\Omega$ is the solid angle covered by the cluster survey, $\ln M_{l,m} = \ln M_{\rm lim}(z_l) + m\Delta \ln M$, and $n(M,z)$ is the mass function given in Eq. (9). Following Lima and Hu [52], we take into account the intrinsic scatter in the relation between true and observed mass, as inferred from a given mass proxy, by the factor $p(M^{\rm ob}|M)$ which is the probability for a given cluster mass with M of having an observed mass $M^{\rm ob}$. Under the assumption of a log–normal distribution for the intrinsic scatter, with variance $\sigma^2_{\ln M}$, the probability is

$$p(M^{\rm ob}|M) = \frac{\exp[-x^2(M^{\rm ob})]}{\sqrt{2\pi\sigma^2_{\ln M}}} \tag{20}$$

where

$$x(M^{\rm ob}) = \frac{\ln M^{\rm ob} - B_{\rm M} - \ln M}{\sqrt{2\sigma^2_{\ln M}}}. \tag{21}$$

With these notations, we parameterize the $M^{\rm ob} - M$ relation, in addition to the intrinsic scatter, by a systematic fractional mass bias $B_{\rm M}$. With this prescription, the final expression for the number count FM is:

$$N_{l,m} = \frac{\Delta\Omega\Delta z}{2} \frac{d^2V}{dz d\Omega} \times \int_0^\infty d\ln M \; n(M,z) \left(\mathrm{erfc}[x_m] - \mathrm{erfc}[x_{m+1}]\right), \tag{22}$$

where $\mathrm{erfc}(x)$ is the complementary error function.

C. Power spectrum

We define the FM for the power spectrum of galaxy clusters as

$$F_{\alpha\beta} = \frac{1}{(2\pi)^2} \sum_{m,n} \sum_{l,i} \frac{\partial \ln P_{\rm h}^{mn}(k_i, z_l)}{\partial p_\alpha} \frac{\partial \ln P_{\rm h}^{mn}(k_i, z_l)}{\partial p_\beta} \times V_{l,i}^{mn,\rm eff} k_i^2 \Delta k \tag{23}$$

where the sum over m, n runs over mass bins, while the sum in l and i runs over intervals in the whole redshift range and wavenumber $0.01\ h\mathrm{Mpc}^{-1} \le k \le 0.1\ h\mathrm{Mpc}^{-1}$ with $\Delta \log_{10} k = 0.017$ respectively. $P_{\rm h}^{mn}(k_i, z_l)$ is the cluster cross-power spectrum for mass bins m and n, calculated for the given redshift and wavenumber through

$$P_{\rm h}^{mn}(k_i, z_l) = b_{\rm eff}^m(z_l) b_{\rm eff}^n(z_l) P_L(k_i, z_l). \tag{24}$$

Here, $b_{\rm eff}^m$ is the mass function weighted effective bias,

$$b_{\rm eff}^m(z) = \frac{\int_0^\infty dM \; n(M,z) b_L(M,z) (\mathrm{erfc}[x_m] - \mathrm{erfc}[x_{m+1}])}{\int_0^\infty dM \; n(M,z) (\mathrm{erfc}[x_m] - \mathrm{erfc}[x_{m+1}])}. \tag{25}$$

The effective volume for mass bins m, n, wave number k_i, and redshift z_l is given by (see App. A)

$$\frac{V^{mn,\rm eff}(k_i, z_l)}{V_0(z_l)} = [P^{mn}(k_i, z_l)]^2 n_m(z_l) n_n(z_l) \times \Big[(n_m P^{mm} + 1)(n_n P^{nn} + 1) + n_m n_n (P^{nm} + \delta^{nm} n_m^{-1})^2 \Big]^{-1}, \tag{26}$$

where $V_0(z)$ is the comoving volume of the redshift slice $[z_l - 0.01, z_l + 0.01]$ covered by the given survey, and $n_m(z_l)$ is the cluster number density for mass bin m at redshift z_l. The effective volume gives the weight carried by each bin in the (z, k) space to the power spectrum Fisher matrix, and hence quantifies the amount of information contained in a given redshift- and k-bin. Fig. 4 shows the redshift and scale dependence of the effective volume for the four cluster surveys. We find that $V_{\rm eff} \lesssim 0.3\, V_0$ for all redshifts and surveys considered, even when not binning in mass, hence the cluster power spectrum is shot-noise dominated for all surveys. As the lower panel of Fig. 4 illustrates, Planck is most limited by shot noise, while SPTpol is least limited, as expected from their respective mass limits and coverage.

D. Calibration parameters

In self-calibrating the true and observed cluster mass (Eq. (21)), we introduce four nuisance parameters which specify the magnitude and redshift-dependence of the fractional mass bias $B_M(z)$ and the intrinsic scatter $\sigma_{\ln M}(z)$. Following [52], we assume the following parametrization:

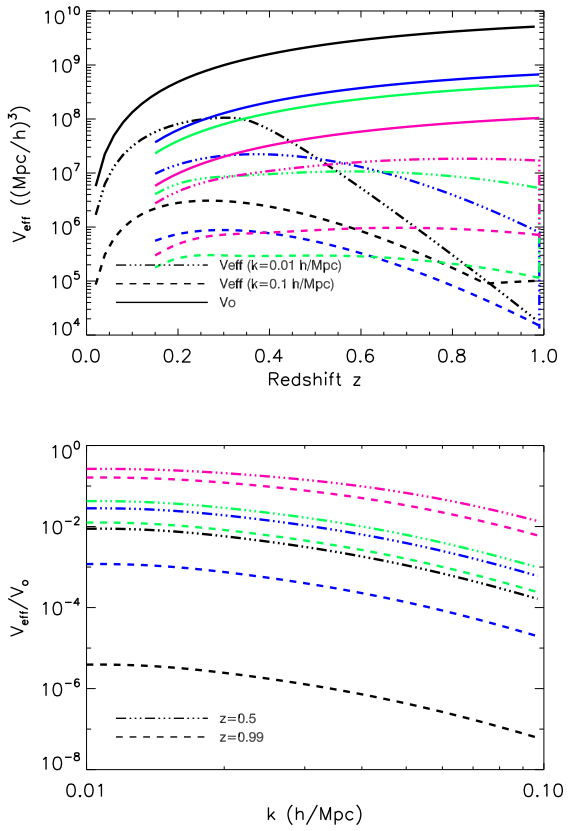

FIG. 4: The dependence on redshift *(top)* and wavenumber *(bottom)* of the effective volume (Eq. (26)) for a single mass bin and each survey: Planck (black), SPT (green), SPTpol (magenta), and ACTpol (blue). The effective volume is a weak function of wavenumber k but strongly depends on the redshift.

$$B_M(z) = B_{M0}(1+z)^{\alpha}$$
$$\sigma_{\ln M} = \sigma_{\ln M,0}(1+z)^{\beta} \qquad (27)$$

Therefore the four nuisance parameters are B_{M0}, α, $\sigma_{\ln M,0}$, and β. A negative value for B_M corresponds to an underestimation of mass. The mass bias accounts for the possibility of a systematic offset in the calibration of the observable mass scaling relation. We adopt fiducial values of $B_{M0} = 0$, $\alpha = 0$, $\sigma_{\ln M} = 0.1$, $\beta = 0$. In deriving the main results, we will not make any assumption on the four nuisance parameters and leave them free to vary. We will study the effect of assuming different priors on the four nuisance parameters on the $f(R)$ constraints in Sec. V D .

E. CMB Prior

In the following, we present results with the Fisher matrix for the Planck CMB temperature power spectrum C_l added to the constraints from cluster counts and power spectrum. We calculate the full CMB fisher matrix with CAMB [53] and method described in [54]. For the Planck experiment, we use the three frequency bands 100, 143 and 217 GHz, and the C_l are calculated up to $l_{\rm max} = 2500$. Our fiducial parameter set for the CMB experiment is, as described in the DETF report [55], $\theta = (n_s, \Omega_b h^2, \Omega_\Lambda, \Omega_m h^2, w_0, A_s, \tau)$, where A_s is the primordial amplitude of scalar perturbations and τ is the optical depth due to reionization. After marginalizing over the optical depth, we transform the Planck CMB fisher matrix to our cluster survey parameter set $\theta' = (n_s, \Omega_b h^2, \Omega_\Lambda, \Omega_m h^2, w_0, \sigma_8)$ by using the appropriate Jacobian matrix. The CMB imposes strong prior on the cosmological parameters. For example, $\Omega_m h^2$ is known to be measured with the CMB power spectrum to an exquisite precision, and this helps in breaking parameter degeneracies in the constraints from cluster surveys. As we shall see in Sec. V, the field amplitude parameter f_{R0} shows degeneracies with some of the cosmological parameters, so that the CMB prior also helps in further constraining f_{R0}.

F. Non-Gaussian likelihood

An inherent assumption in the Fisher matrix approach is that the likelihood can be approximated as Gaussian around its maximum; in other words, that one can do a reasonably accurate Taylor expansion of $\ln \mathfrak{L}$ in all parameters. Unfortunately, this is not the case for the parameter f_{R0}, as the derivatives of the likelihood with respect to f_{R0} diverge at the fiducial value $f_{R0} = 0$ (see Fig. 5 in [15]). Thus, we choose the Compton wavelength λ_{C0} as a parameter instead of f_{R0}, where for the $f(R)$ model and fiducial cosmology considered here,

$$\lambda_{C0} \approx 32.53\sqrt{\frac{|f_{R0}|}{10^{-4}}}\ \text{Mpc}. \qquad (28)$$

With this choice, $\ln \mathfrak{L}$ becomes analytic at the fiducial value $\lambda_{C0} = 0$. Specifically, we calculate the derivatives numerically as

$$\frac{d\ln\mathfrak{L}}{d\lambda_{C0}} = \frac{\ln\mathfrak{L}(\lambda_{C0}) - \ln\mathfrak{L}(0)}{\lambda_{C0}}, \qquad (29)$$

where λ_{C0} is the Compton wavelength evaluated at the chosen step size $f_{R0} = \Delta f_{R0}$ through Eq. (28), and $\mathfrak{L}$ denotes the likelihood from either dN/dz or $P(k)$. Unfortunately, the likelihood is still strongly non-Gaussian in the direction of λ_{C0}, and the constraints depend on the step size Δf_{R0} chosen to evaluate the Fisher matrix elements in Eq. (17). In principle, one would have to

evaluate the full likelihood with a MCMC approach, and then perform a marginalization to obtain proper forecasted constraints. Here, we opt instead for a simpler approach. We evaluate the Fisher matrix for a range of step sizes Δf_{R0}, and then quote the constraints for which $\sigma(f_{R0}) = \Delta f_{R0}$ is satisfied. One can easily show that this gives the correct answer in the ideal case where the likelihood is Gaussian in all other parameters. Note that while we always use λ_{C0} as parameter in the Fisher matrix, we will quote constraints in terms of f_{R0} in order to facilitate comparison with the literature, using λ_{C0} only to show parameter degeneracies.

V. RESULTS

We begin by discussing constraints from number counts (Sec. V A) and power spectrum (Sec. V B) separately, before moving on to combined constraints (Sec. V C) and the impact of external priors on the nuisance parameters (Sec. V D).

A. Number counts

As discussed in Sec. IV F, the Fisher constraints depend on the value of Δf_{R0} adopted to evaluate the numerical derivatives in the Fisher matrix. Fig. 5 shows the projected constraints for the different surveys as a function of Δf_{R0}. The sharp upturn at $\Delta f_{R0} \sim 3\times10^{-5}$ (SPT and ACTPol), $\Delta f_{R0} \sim 2\times10^{-5}$ (SPTPol) and $\Delta f_{R0} \sim 9\times10^{-6}$ (Planck) signals the transition to the chameleon-screened regime, where the mass function enhancement becomes negligible [22]. The shape of this transition depends on the mass limits of the different surveys, as more massive halos are screened for larger values of f_{R0}. The figure clearly shows that, with number counts alone, constraints cannot be tighter than $\sigma_{f_{R0}} \sim 10^{-5}$. Nevertheless, this still constitutes an order of magnitude in improvement over current constraints. It should also be noted that the use of the dynamical mass in the calculations leads to a significant improvement in constraints in the large-field regime where the chameleon mechanism is not active.

The precise constraints obtained at the intersection $\sigma_{f_{R0}} = \Delta f_{R0}$ are listed in Tab. I, along with the step size used for each survey. The relative constraining power of the different surveys can easily be interpreted by looking at $\Delta N/N$ shown in Fig. 2. The best survey to constrain $f(R)$ with number counts is Planck which shows prominent deviations in $\Delta N/N$ at low redshift, and yields a 68% CL constraint of $\sigma_{f_{R0}} = 2\times10^{-5}$. Although SPTpol shows significant differences in number counts out to large redshifts, the relatively small survey volume compared to Planck limits the performance in constraining $f(R)$ to $\sigma_{f_{R0}} \simeq 3\times10^{-5}$. It is interesting to notice that while their overall performance is similar, the constraints leverage on clusters in almost disjoint redshift ranges. Therefore these surveys provide complementary information on $f(R)$ constraints from number counts, making the overall result less susceptible to specific issues related to either low or high redshift clusters. An investigation of whether the combination of both cluster samples yields a significant improvement on the expected $f(R)$ constraints would be worthwhile, but is beyond the scope of this paper. The other two surveys also present results highly competitive with current constraints, and not very different from SPTPol ($\sigma_{f_{R0}} = 3\times10^{-5}$). A better investigation with a proper likelihood would be necessary in order to make more precise statements.

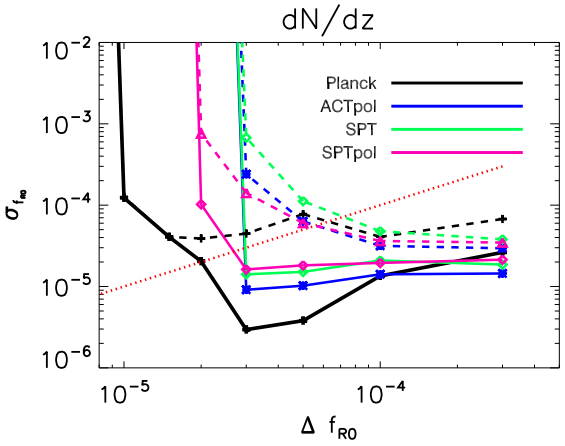

FIG. 5: Fully marginalized 68% confidence level (CL) constraints on f_{R0} from the number count of clusters only (using Planck CMB priors), as a function of the step size Δf_{R0}, for the surveys considered in this paper. The red dotted line indicates $\sigma_{f_{R0}} = \Delta f_{R0}$. For a given survey, the intersection of this line with the predicted constraints yields the final expected constraint (Sec. IV F). Solid (dashed) lines represent the case when dynamical mass is (is not) considered. The sharp upturn at $\Delta f_{R0} \lesssim 5\times10^{-5}$ is due to the chameleon mechanism.

B. Power spectrum

Fig. 6 shows the constraints from the clustering of clusters alone as a function of step size. The constraints generally worsen as the step size decreases to very small values. This is because the likelihood around the fiducial model (ΛCDM) scales as ${\lambda_{C0}}^a$, where $a > 1$, and hence the derivatives go to zero as the step size decreases. However, constraints do not worsen dramatically as the step size crosses the chameleon threshold, because the modification to the halo bias in $f(R)$ persists even if the halos are chameleon screened [22]. Furthermore, the deviations in the matter power spectrum on small scales also persist for field values $f_{R0} < 10^{-5}$. As expected, the use of the dynamical mass does not affect the constraints for small field values where the entire cluster sample is chameleon

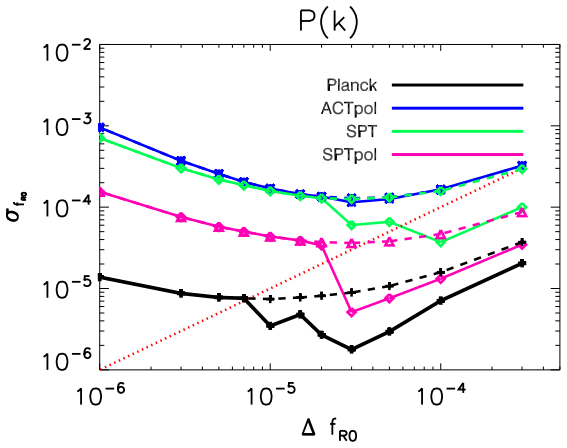

FIG. 6: Same as Fig. 5, but from the power spectrum of clusters only (using Planck CMB priors).

screened.

The constraints from power spectrum only are summarized in the second column of Tab. I. For Planck (as well as marginally for SPTPol) the constraint on f_{R0} from the cluster power spectrum is tighter than that from the abundance only. This is mainly because the power spectrum retains sensitivity to $f(R)$ effects even when the halos are chameleon screened. For ACTPol and SPT the power spectrum yields slightly less constraining power than number counts, as the disadvantage of not having all-sky coverage is not compensated by the relatively low mass threshold.

In order to investigate what cluster redshift range contributes to the f_{R0} constraints, we the constraints (for $\Delta f_{R0} = 7 \times 10^{-6}$ fixed) as function of the maximum cluster redshift considered in Fig. 7. For surveys with mass limits which decrease with redshift, i.e. SPT and SPTpol, constraints improve up to $z_{\rm max} = 1$, while for Planck all the information is derived from clusters below $z \approx 0.3$, and for ACT the constraining power comes from clusters below $z \approx 0.5$. It is especially interesting to compare results from ACTpol and SPT, which detect a comparable number of clusters overall but with a different redshift distribution. Fig. 2 shows that ACTpol has a significantly higher number of clusters than SPT out to $z \approx 0.5$, and a lower mass limit out to $z \approx 0.3$. Yet the constraints from the cluster power spectrum are worse for ACTpol than SPT, due to the contribution from $z > 0.5$ clusters for SPT (Fig. 7). How well each survey can realize their potential constraining power clearly depends on the precise $M_{\rm lim}(z)$ achieved in the final cluster sample.

C. Combined constraints

Fig. 8 shows constraints on f_{R0} when combining both number counts and clustering, as a function of the step

TABLE I: Marginalized constraints (68% confidence level) from the two cluster probes dN/dz and $P(k)$, as well as the combination of both for the four SZ surveys. The results are combined with forecasted constraints from the Planck CMB. We also indicate the step size Δf_{R0} used for each survey and probe. The results reported as approximate values refer to the case in which the constraints do not match any of the explicitly evaluated step size.

Parameter	dN/dz	$P(k)$	$dN/dz + P(k)$
		Planck	
Δf_{R0}	2×10^{-5}	7×10^{-6}	5×10^{-6}
f_{R0}	2.04×10^{-5}	7.58×10^{-6}	5.13×10^{-6}
$\Omega_M h^2$	1.10×10^{-3}	1.09×10^{-3}	1.07×10^{-3}
Ω_Λ	0.17	9.84×10^{-2}	3.18×10^{-2}
σ_8	6.31×10^{-3}	6.26×10^{-3}	6.15×10^{-3}
$\Omega_b h^2$	1.31×10^{-4}	1.30×10^{-4}	1.29×10^{-4}
n_s	3.33×10^{-3}	3.30×10^{-3}	3.27×10^{-3}
w_0	0.64	0.36	0.11
w_a	2.34	13.10	1.11
		ACTpol	
Δf_{R0}	3×10^{-5}	3×10^{-4}	2×10^{-5}
f_{R0}	$\sim 3 \times 10^{-5}$	3.23×10^{-4}	$\sim 3 \times 10^{-5}$
$\Omega_M h^2$	1.10×10^{-3}	1.10×10^{-3}	1.09×10^{-3}
Ω_Λ	0.17	0.17	0.13
σ_8	6.31×10^{-3}	6.32×10^{-3}	6.27×10^{-3}
$\Omega_b h^2$	1.31×10^{-4}	1.31×10^{-4}	1.31×10^{-4}
n_s	3.33×10^{-3}	3.33×10^{-3}	3.30×10^{-3}
w_0	0.65	0.64	0.48
w_a	2.18	11.50	1.45
		SPT	
Δf_{R0}	3×10^{-5}	5×10^{-5}	2×10^{-5}
f_{R0}	$\sim 3 \times 10^{-5}$	6.60×10^{-5}	$\sim 3 \times 10^{-5}$
$\Omega_M h^2$	1.10×10^{-3}	1.09×10^{-3}	1.09×10^{-3}
Ω_Λ	0.17	8.82×10^{-2}	6.47×10^{-2}
σ_8	6.31×10^{-3}	6.28×10^{-3}	6.26×10^{-3}
$\Omega_b h^2$	1.31×10^{-4}	1.31×10^{-4}	1.31×10^{-4}
n_s	3.33×10^{-3}	3.30×10^{-3}	3.29×10^{-3}
w_0	0.65	0.31	0.23
w_a	2.28	5.11	0.94
		SPTpol	
Δf_{R0}	2×10^{-5}	2×10^{-5}	2×10^{-5}
f_{R0}	$\sim 3 \times 10^{-5}$	$\sim 3 \times 10^{-5}$	2.04×10^{-5}
$\Omega_M h^2$	1.10×10^{-3}	1.09×10^{-3}	1.09×10^{-3}
Ω_Λ	0.17	6.06×10^{-2}	3.63×10^{-2}
σ_8	6.32×10^{-3}	6.26×10^{-3}	6.24×10^{-3}
$\Omega_b h^2$	1.31×10^{-4}	1.31×10^{-4}	1.30×10^{-4}
n_s	3.33×10^{-3}	3.29×10^{-3}	3.29×10^{-3}
w_0	0.62	0.22	0.14
w_a	2.16	2.82	0.88

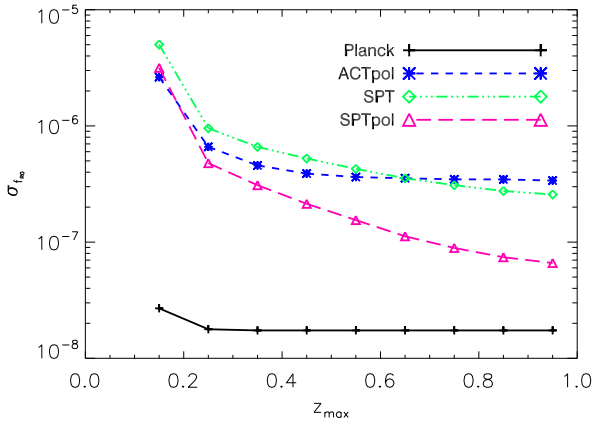

FIG. 7: Fully marginalized constraints on f_{R0} from the power spectrum of clusters only, as a function of maximum cluster redshift $z_{\rm max}$. $\Delta f_{R0} = 7 \times 10^{-6}$ was used for all values shown here.

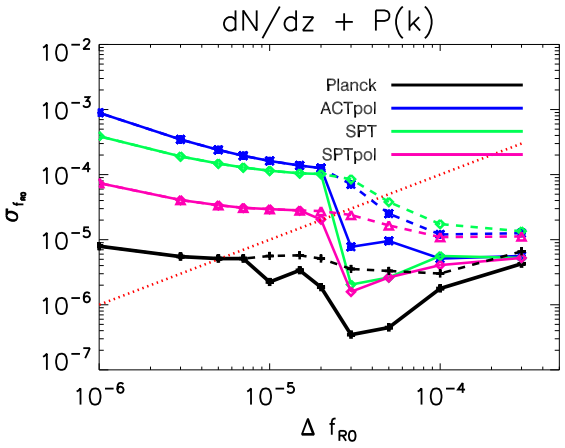

FIG. 8: Combined $dN/dz + P(k)$ 68% CL marginalized constraints on f_{R0} as a function of the step size Δf_{R0} for the different surveys. As in Fig. 5, the red dotted line shows the identity $\sigma_{f_{R0}} = \Delta f_{R0}$.

size Δf_{R0}. The dependence on Δf_{R0} is similar to the case of power spectrum-only and number counts-only constraints at small and large step size respectively. Combining the two probes helps to break degeneracies and better constrain the nuisance parameters. As a result, the constraints on f_{R0} show improvements with respect to those derived from power spectrum or number counts alone (third column in Tab. I). While Planck reaches a constraint of $\sigma_{R0} \approx 5 \times 10^{-6}$, ACTpol, SPT and SPTPol achieve $2-3 \times 10^{-5}$. Among the four surveys, the Planck survey thus yields the tightest constraints regardless of which cluster probe is being used. The relative merit of the Planck survey is due to its large area, which allows to detect massive clusters on the whole sky, and its ability to detect low redshift clusters. Fig. 2 shows that in the small-field regime ($f_{R0} \sim 10^{-5}$), the low redshift clusters drive the constraints for Planck, while low mass clusters do so for SPTPol.

Up to now, we presented results with conservative mass limits, i.e. clusters are expected to be detected with $S/N \geq 5$ for all the surveys. We also examined improvements in the constraint $\sigma_{f_{R0}}$ when using more optimistic mass limits for each survey, according to what is outlined in section Sec. II. For all surveys, the constraints from number counts only are hardly affected, since they are mainly set by the chameleon threshold. In each case, the larger cluster sample does improve the power spectrum constraints. However, only for Planck does this yield a significant improvement in the combined constraints (by a factor of 1.5 to 3×10^{-6}), while for ACTpol, SPT, and SPTpol, the improvement in combined constraints is marginal.

Fig. 9 illustrates the most important degeneracies of λ_{C0} with standard cosmological parameters for the Planck survey. Here, we show λ_{C0} instead of f_{R0} for purposes of presentation. The most prominent degeneracies are with the amount and equation of state of dark energy (Ω_Λ, w_o and w_a). Clearly, the combination of both observables yields a significant reduction in degeneracies in all cases. The degeneracy with dark energy parameters also explains why the combined constraints on f_{R0} are slightly better for SPT than for ACTPol, even though the constraints from number counts and clustering separately are very similar for the two surveys. By probing higher redshifts more effectively, SPT is able to better break degeneracies with dark energy parameters.

Constraints on modified gravity show little with the power spectrum normalization (see Fig. 9). This is due to the fact that the high number of clusters detected allows for good characterization of the shape of the mass function beyond its overall normalization. Similar but somewhat weaker degeneracies are present for the other surveys.

D. Uncertainties in scatter of mass observable relations

Throughout this work, we have assumed a functional form for the scaling relations and then allowed the data to calibrate the parameters that characterize it. This procedure is possible thanks to the large number of clusters that are expected to be detected in these surveys. Current strategies for deriving constraints from cluster surveys, however, rely on the calibration of scaling relations as obtained by a small subset of well studied clusters. In general, allowing more freedom to the scaling relation parameters may avoid biases induced by incorrect scaling relations but can also result in a degradation of the final result. In order to investigate the degradation of $\sigma_{f_{R0}}$ due to this self-calibration, we repeat the forecasts assuming different priors on the four "nuisance" parameters. The

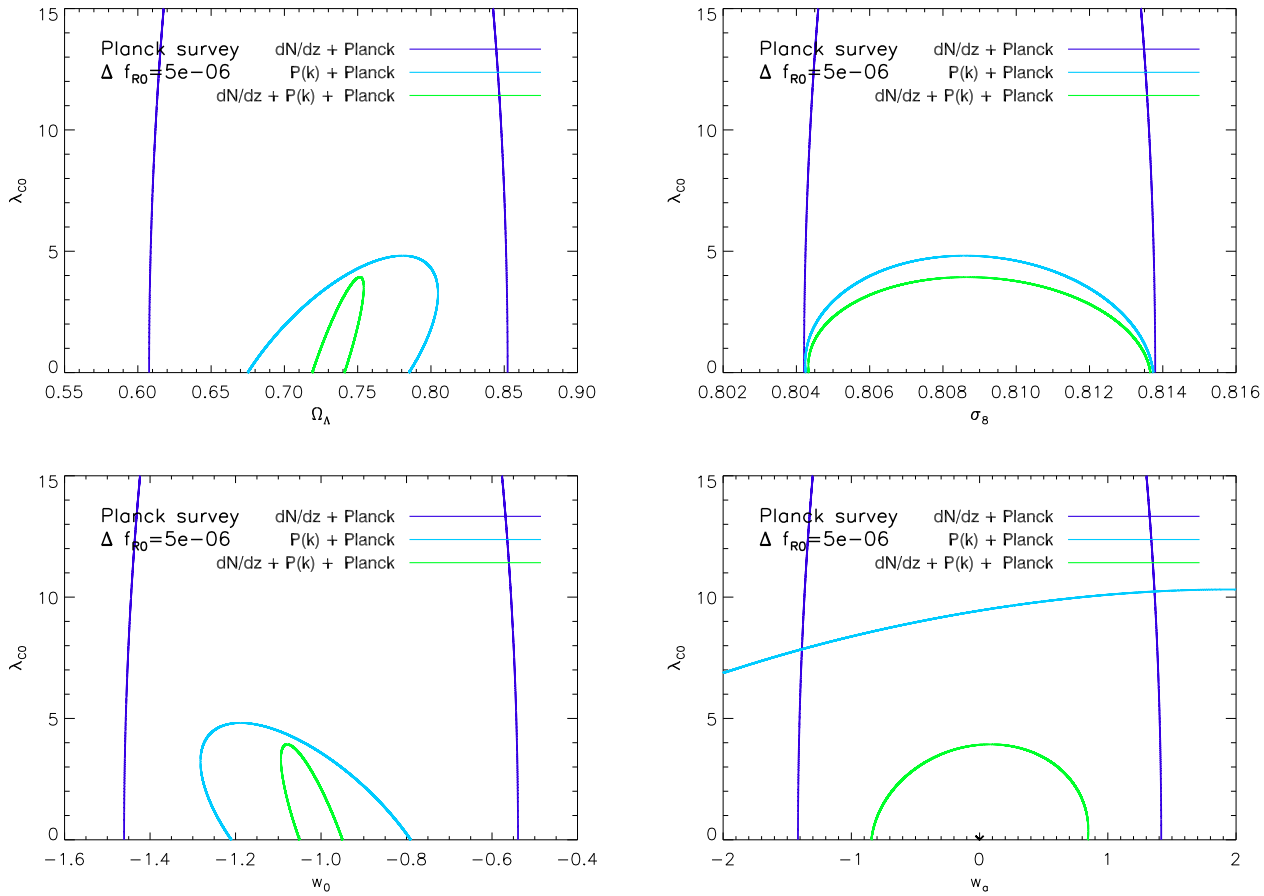

FIG. 9: Joint constraints on the Compton wavelength λ_{C0} (in Mpc; see Eq. (28)) and *(counterclockwise from top left)* Ω_Λ, σ_8, w_o, and w_a. All curves denote 68% confidence level, and are for number counts only (blue), power spectrum only (cyan), and combination of the two (green). The results are shown for the Planck survey with $\Delta f_{R0} = 5 \times 10^{-6}$.

result is summarized in Tab. II for the number counts, clustering, and combined, and for the four surveys.

Here, the "weak prior" case assumes priors on the nuisance parameters of $\Delta B_{M,0} = 0.05$ and $\Delta\alpha = 1$, as well as $\Delta\sigma_{M,0} = 0.1$ and $\Delta\beta = 1$, as suggested by comparison between X-ray and lensing cluster mass measurement (e.g., the XMM-Newton measurements presented in [56]). The combined constraints on f_{R0} are smaller than those for the default, no prior case, by about 25% for Planck, 80% for ACTpol, and 50% for SPT and SPTpol. The most prominent improvements are seen in number counts only constraints (e.g. a factor 3.8 for SPT).

The "strong prior" case assumes that all four nuisance parameters are fixed at their fiducial values. This assumption, which is anyway not realistic, would lead to improvements of about one order of magnitude with respect to the self-calibration results.

This result suggests that although self-calibration does not in general lead to major degradations in the constraints, good prior information on normalization and scatter in the mass-observable relation can improve constraints considerably in partiuclar for the ACTpol and SPT/SPTpol surveys.

On the other hand, it is important to keep in mind that self-calibration relies on a specific parametrization of the mass-observable relation and its scatter, and external measurements are important to validate these assumptions. As a worst-case scenario, we also considered the case of a single mass bin for each survey, i.e. neglecting all mass information on individual clusters. The fully marginalized, combined constraints on f_{R0} (without any priors on bias and scatter) worsen by approximately a factor of two for Planck and ACTpol. On the other hand, both SPT and SPTpol constraints degrade by only $\sim 10\%$, since these surveys have a large lever arm in redshift. While these constraints are considerably worse than when using mass bins, the Planck, SPT, and SPTpol constraints with a single mass bin still improve over current upper limits.

TABLE II: Relative improvement in constraints on f_{R0}, i.e. $\sigma^{\rm no\ prior}_{f_{R0}}/\sigma^{\rm weak}_{f_{R0}}$, when including weak priors on the mass-observable relation (see text). In each case, Δf_{R0} is that given in Tab. I for the corresponding survey/probe.

Survey	$f_{R0}(10^{-6})$			λ_{C0} (Mpc/h)		
	dN/dz	$P(k)$	dN/dz $+P(k)$	dN/dz	$P(k)$	dN/dz $+P(k)$
			weak			
Planck	1.00	1.05	1.26	1.02	1.02	1.12
ACTpol	2.14	1.82	1.91	1.01	1.18	1.38
SPT	3.80	1.12	1.48	1.03	1.01	1.21
SPTpol	1.29	1.0	1.45	1.13	1.00	1.21

VI. DISCUSSION

It is worth comparing our forecasted constraints on f_{R0} with those obtained in Schmidt et al. [15] (Lombriser et al. [16] obtained similar constraints). By combining 49 Chandra X-ray clusters and using geometric constraints from CMB, supernovae, H_0, and BAO, they found an upper limit of $f_{R0} < 1.4 \times 10^{-4}$ (95% CL), including only the statistical error. Our forecasted constraints are tighter by a factor of $\sim 3-4$ (ACTpol, SPT, SPTPol) and ~ 15 (Planck), respectively. The main reasons for the tighter constraints are: the significantly larger cluster samples yielded by these surveys, the use of the dynamical mass (which improves number count constraints), and the inclusion of the clustering of clusters as an observable. As shown in Sec. V, the latter in fact provides the dominant constraining power for these surveys in the small field limit.

Furthermore, the constraints in [15] are dominated by the systematic uncertainty in the cluster mass scale, and including this systematic increases the upper limit to $f_{R0} \lesssim 3 \times 10^{-4}$. The constraints presented here are marginalized over the cluster mass scale, and hence already include this systematic. Indeed, the combination of power spectrum and number counts is essential in order to realize self-calibration without loosing constraining power.

One interesting finding of our study is that the chameleon screening mechanism, a necessary ingredient in this modified gravity model in order to satisfy Solar System constraints, has a qualitative impact on the constraints. In particular, the number counts by themselves cannot push constraints below $f_{R0} \sim 10^{-5}$ due to this effect, while they yield the tightest constraints for larger field values. Similarly, the importance of the dynamical mass effect is controlled by the chameleon threshold. This is expected to hold for other modified gravity scenarios as well, as long as the respective screening mechanism depends mainly on the host halo mass (or potential well) of the cluster. On the other hand, screening mechanisms that mainly depend on the average interior density, such as the Vainshtein mechanism employed in braneworld and galileon models, will show a qualitatively different behavior [49, 57] (see [58] for a study of the related symmetron mechanism). For such models, the utility of number counts will not be limited to certain parameter ranges. Thus, taking into account the screening mechanism is crucial for obtaining realistic constraints on any viable modified gravity model, both for forecasts and when using actual data.

All of the surveys considered here reach the limit set by the chameleon mechanism on the constraints from number counts. The Planck survey achieves the tightest constraints both due to its large volume, which reduces the sample variance especially in the cluster power spectrum, and due to its ability to detect clusters at $z < 0.15$. For example, if we limit the Planck cluster sample to $z \geq 0.15$, the combined constraints in f_{R0} degrade by a factor of three to $\sim 2 \times 10^{-5}$. We thus expect that significant improvements in constraining power are achievable for ground-based SZ surveys if the minimum cluster redshift can be reduced.

Several improvements upon our treatment here are possible. First, our model for the $f(R)$ effects on mass function and bias of halos is conservative. In order to investigate this, we repeated the forecast using the standard as opposed to modified spherical collapse parameters in the model prediction [22]. In case of the Planck survey, the fully marginalized, combined constraint is tightened by a factor of $5-6$, constraining f_{R0} to less than 10^{-6}. This prescription overestimates the $f(R)$ effects in the small field regime ($f_{R0} \lesssim 10^{-5}$) and thus leads to overly optimistic constraints. Nevertheless, the improvement in constraints signals that it is worth developing a more accurate model for the $f(R)$ effects on halo mass function and bias (e.g., along the lines of [59]). Given the importance of the cluster power spectrum in the constraints, an accurate model for the modified halo bias will be crucial. Furthermore, a model for the cluster power spectrum on mildly non-linear scales would also lead to tighter constraints by allowing $k_{\rm max}$ to be increased above the value of $0.1h$/Mpc adopted here.

VII. CONCLUSIONS

The large cluster samples expected from current and upcoming SZ surveys can be exploited to place tight constraints on modifications to gravity. We have shown that the Planck cluster sample will allow for more than one order of magnitude improvement in constraints on the field parameter f_{R0} over current observational constraints, even when marginalizing over the expansion history (parametrized by w_0, w_a) and bias and scatter in the mass-observable relation. Similarly, SPT, SPTPol and ACTPol should provide improvements of about a factor 3–4. Using number counts only, the Planck cluster catalog should be able to reduce errors to $\sigma_{f_{R0}} = 2 \times 10^{-5}$

in the near future. The inclusion of the cluster power spectrum as a probe greatly improves results especially in the small field limit. The best constraint we obtain is for Planck (combined constraints, $\sigma_{f_{R0}} = 5\times10^{-6}$) and is mainly driven by the power spectrum. These constraints push into the regime not ruled out by Solar System tests [19]. Even with self-calibration, a good understanding of the cluster selection function will be necessary to realize this potential however. On the theoretical side, a better description of the modified gravity effects on halo mass function and bias should allow for further improvements. In addition, the use of a proper likelihood function would constitute an important validation of the results obtained here with the Fisher matrix approximation.

Acknowledgments

EP and NM acknowledge support from NSF grant AST-0649899. EP and DM were partially supported by NASA grant NNX07AH59G. EP also acknowledges support from JPL-Planck subcontract 1290790. She would like to thank the hospitality of the Aspen Center for Physics for hospitality during the preparation of this work. FS would like to thank Wayne Hu for helpful discussions. FS is supported by the Gordon and Betty Moore foundation at Caltech.

Appendix A: Covariance of Cluster Power Spectra

In this appendix we derive the Fisher matrix element for the cross- and auto-power spectra of clusters binned in mass. Let $P^{mn}(k)$ denote the cross-power spectrum between mass bins m and n. In this section we will suppress the explicit redshift-dependence for clarity. The variance of the cross-power spectrum measured in a narrow k range is given by

$$\sigma^2\left(P^{mn}(k)\right) = \frac{1}{N_{\rm mod}}\left[\left(P^{mm}(k)+\frac{1}{n_m}\right)\left(P^{nn}(k)+\frac{1}{n_j}\right) + \left(P^{mn}(k)+\frac{\delta^{mn}}{n_m}\right)^2\right]. \quad \text{(A1)}$$

Here, n_m denotes the comoving number density of clusters in mass bin i, and the number of modes is given by

$$N_{\rm mod} = \frac{1}{2}\frac{V\,k^2\Delta k}{2\pi^2}, \quad \text{(A2)}$$

where the factor of $1/2$ in front accounts for the fact that the density field is real, reducing the number of independent modes by one half. This factor is sometimes neglected in the literature. The volume is given by

$$V(z) = \Omega_s\chi^2(z)\frac{c}{H(z)}\Delta z. \quad \text{(A3)}$$

Using this, we can derive the general power spectrum Fisher matrix as

$$F_{\alpha\beta} = \frac{1}{4\pi^2}\sum_{i,j}\sum_{l,m}\left[\frac{\partial \ln P^{mn}(k_m,z_l)}{\partial p_\alpha}\frac{\partial \ln P^{mn}(k_m,z_l)}{\partial p_\beta} \times V^{mn,\rm eff}(k_m,z_l)k_m^2\Delta k\right], \quad \text{(A4)}$$

with

$$\frac{V^{mn,\rm eff}(k_i,z_l)}{V_0(z_l)} = P^{mn}(k_i,z_l)]^2 n_m(z_l)n_n(z_l) \times\left[(n_mP^{mm}+1)(n_nP^{nn}+1)+n_mn_n(P^{nm}+\delta^{nm}n_m^{-1})^2\right]^{-1},$$

where all quantities in the denominator are evaluated at k_m and z_l. This is Eq. (26).

[1] J. L. Tinker, A. V. Kravtsov, A. Klypin, K. Abazajian, M. S. Warren, G. Yepes, S. Gottlober, and D. E. Holz, ArXiv e-prints **803** (2008), 0803.2706.

[2] R. Sheth and B. Tormen, MNRAS **308**, 119 (1999).

[3] P. T. P. Viana and A. R. Liddle, MNRAS **303**, 535 (1999).

[4] E. Pierpaoli, D. Scott, and M. White, MNRAS **325**, 77 (2001), arXiv:astro-ph/0010039.

[5] E. Pierpaoli, S. Borgani, D. Scott, and M. White, MNRAS **342**, 163 (2003), arXiv:astro-ph/0210567.

[6] S. Borgani, P. Rosati, P. Tozzi, S. A. Stanford, P. R. Eisenhardt, C. Lidman, B. Holden, R. Della Ceca, C. Norman, and G. Squires, Astrophys. J. **561**, 13 (2001), arXiv:astro-ph/0106428.

[7] S. W. Allen, R. W. Schmidt, A. C. Fabian, and H. Ebeling, MNRAS **342**, 287 (2003), arXiv:astro-ph/0208394.

[8] E. Pierpaoli, in *Astrophysics and Space Science Library*, edited by M. Plionis (2004), vol. 301 of *Astrophysics and Space Science Library*, pp. 93–+.

[9] S. W. Allen, R. W. Schmidt, and S. L. Bridle, MNRAS **346**, 593 (2003), arXiv:astro-ph/0306386.

[10] A. Vikhlinin, A. V. Kravtsov, R. A. Burenin, H. Ebeling, W. R. Forman, A. Hornstrup, C. Jones, S. S. Murray, D. Nagai, H. Quintana, et al., Astrophys. J. **692**, 1060 (2009), 0812.2720.

[11] M. C. Martino, H. F. Stabenau, and R. K. Sheth, Phys. Rev. D **79**, 084013 (2009), 0812.0200.

[12] A. Diaferio and L. Ostorero, MNRAS **393**, 215 (2009), 0808.3707.

[13] B. Jain and J. Khoury, Annals of Physics **325**, 1479 (2010), 1004.3294.

[14] T. Clifton, P. G. Ferreira, A. Padilla, and C. Skordis, ArXiv e-prints (2011), 1106.2476.

[15] F. Schmidt, A. Vikhlinin, and W. Hu, Phys. Rev. **D80**, 083505 (2009), 0908.2457.

[16] L. Lombriser, A. Slosar, U. Seljak, and W. Hu (2010), 1003.3009.

[17] D. Rapetti, S. W. Allen, A. Mantz, and H. Ebeling, MNRAS **406**, 1796 (2010), 0911.1787.

[18] T. P. Sotiriou and V. Faraoni, Rev. Mod. Phys. **82**, 451 (2010), 0805.1726.

[19] W. Hu and I. Sawicki, Phys. Rev. D **76**, 064004 (2007), arXiv:0705.1158.

[20] H. Oyaizu, Phys. Rev. **D78**, 123523 (2008), 0807.2449.

[21] H. Oyaizu, M. Lima, and W. Hu, Phys. Rev. **D78**, 123524 (2008), 0807.2462.

[22] F. Schmidt, M. V. Lima, H. Oyaizu, and W. Hu, Phys. Rev. **D79**, 083518 (2009), 0812.0545.

[23] G.-B. Zhao, B. Li, and K. Koyama, Phys. Rev. D **83**, 044007 (2011), 1011.1257.

[24] R. Williamson, B. A. Benson, F. W. High, K. Vanderlinde, P. A. R. Ade, K. A. Aird, K. Andersson, R. Armstrong, M. L. N. Ashby, M. Bautz, et al., Astrophys. J. **738**, 139 (2011), 1101.1290.

[25] K. Vanderlinde, T. M. Crawford, T. de Haan, J. P. Dudley, L. Shaw, P. A. R. Ade, K. A. Aird, B. A. Benson, L. E. Bleem, M. Brodwin, et al., Astrophys. J. **722**, 1180 (2010), 1003.0003.

[26] T. A. Marriage, V. Acquaviva, P. A. R. Ade, P. Aguirre, M. Amiri, J. W. Appel, L. F. Barrientos, E. S. Battistelli, J. R. Bond, B. Brown, et al., Astrophys. J. **737**, 61 (2011), 1010.1065.

[27] Planck Collaboration, P. A. R. Ade, N. Aghanim, M. Arnaud, M. Ashdown, J. Aumont, C. Baccigalupi, A. Balbi, A. J. Banday, R. B. Barreiro, et al., ArXiv e-prints (2011), 1101.2024.

[28] Planck Collaboration, N. Aghanim, M. Arnaud, M. Ashdown, F. Atrio-Barandela, J. Aumont, C. Baccigalupi, A. Balbi, A. J. Banday, R. B. Barreiro, et al., ArXiv e-prints (2011), 1106.1376.

[29] M. Birkinshaw, Physics Reports **310**, 97 (1999), arXiv:astro-ph/9808050.

[30] S. Ameglio, S. Borgani, E. Pierpaoli, K. Dolag, S. Ettori, and A. Morandi, MNRAS **394**, 479 (2009), 0811.2199.

[31] E. Rasia, P. Mazzotta, S. Borgani, L. Moscardini, K. Dolag, G. Tormen, A. Diaferio, and G. Murante, ApJ **618**, L1 (2005), arXiv:astro-ph/0409650.

[32] D. Nagai, A. Vikhlinin, and A. V. Kravtsov, Astrophys. J. **655**, 98 (2007), arXiv:astro-ph/0609247.

[33] R. Piffaretti and R. Valdarnini, A & A **491**, 71 (2008), 0808.1111.

[34] J. Melin, J. G. Bartlett, and J. Delabrouille, A & A **459**, 341 (2006), arXiv:astro-ph/0602424.

[35] N. Sehgal, H. Trac, K. Huffenberger, and P. Bode, Astrophys. J. **664**, 149 (2007), arXiv:astro-ph/0612140.

[36] B. Malte Schäfer and M. Bartelmann, MNRAS **377**, 253 (2007), arXiv:astro-ph/0602406.

[37] K. Vanderlinde, T. M. Crawford, T. de Haan, J. P. Dudley, L. Shaw, P. A. R. Ade, K. A. Aird, B. A. Benson, L. E. Bleem, M. Brodwin, et al., Astrophys. J. **722**, 1180 (2010), 1003.0003.

[38] M. D. Niemack, P. A. R. Ade, J. Aguirre, F. Barrientos, J. A. Beall, J. R. Bond, J. Britton, H. M. Cho, S. Das, M. J. Devlin, et al., in *Society of Photo-Optical Instrumentation Engineers (SPIE) Conference Series* (2010), vol. 7741 of *Society of Photo-Optical Instrumentation Engineers (SPIE) Conference Series*, 1006.5049.

[39] S. Nojiri and S. D. Odintsov, Int.J.Geom.Meth.Mod.Phys. **4**, 06 (2006), hep-th/0601213.

[40] S. M. Carroll, V. Duvvuri, M. Trodden, and M. S. Turner, Phys. Rev. **D70**, 043528 (2004), astro-ph/0306438.

[41] S. Nojiri and S. D. Odintsov, Phys. Rev. **D68**, 123512 (2003), hep-th/0307288.

[42] S. Capozziello, S. Carloni, and A. Troisi, Recent Res. Dev. Astron. Astrophys. **1**, 625 (2003), astro-ph/0303041.

[43] J. Khoury and A. Weltman, Phys. Rev. D **69**, 044026 (2004), arXiv:astro-ph/0309411.

[44] Y.-S. Song, W. Hu, and I. Sawicki, Phys. Rev. D **75**, 044004 (2007), arXiv:astro-ph/0610532.

[45] S. Ferraro, F. Schmidt, and W. Hu, Phys. Rev. D **83**, 063503 (2011), 1011.0992.

[46] J. F. Navarro, C. S. Frenk, and S. D. M. White, Astrophys. J. **490**, 493 (1997), astro-ph/9611107.

[47] W. Hu and A. V. Kravtsov, Astrophys. J. **584**, 702 (2003), arXiv:astro-ph/0203169.

[48] J. S. Bullock, T. S. Kolatt, Y. Sigad, R. S. Somerville, A. V. Kravtsov, A. A. Klypin, J. R. Primack, and A. Dekel, MNRAS **321**, 559 (2001), arXiv:astro-ph/9908159.

[49] F. Schmidt, Phys. Rev. D **81**, 103002 (2010), 1003.0409.

[50] J. L. Tinker, B. E. Robertson, A. V. Kravtsov, A. Klypin, M. S. Warren, G. Yepes, and S. Gottlöber, Astrophys. J. **724**, 878 (2010), 1001.3162.
[51] E. Komatsu, K. M. Smith, J. Dunkley, C. L. Bennett, B. Gold, G. Hinshaw, N. Jarosik, D. Larson, M. R. Nolta, L. Page, et al., ApJS **192**, 18 (2011), 1001.4538.
[52] M. Lima and W. Hu, Phys. Rev. D **72**, 043006 (2005), astro-ph/0503363.
[53] A. Lewis, A. Challinor, and A. Lasenby, Astrophys. J. **538**, 473 (2000), arXiv:astro-ph/9911177.
[54] J. R. Pritchard and E. Pierpaoli, Phys. Rev. D **78**, 065009 (2008), 0805.1920.
[55] A. Albrecht, G. Bernstein, R. Cahn, W. L. Freedman, J. Hewitt, W. Hu, J. Huth, M. Kamionkowski, E. W. Kolb, L. Knox, et al., ArXiv Astrophysics e-prints (2006), arXiv:astro-ph/0609591.
[56] Y.-Y. Zhang, N. Okabe, A. Finoguenov, G. P. Smith, R. Piffaretti, R. Valdarnini, A. Babul, A. E. Evrard, P. Mazzotta, A. J. R. Sanderson, et al., Astrophys. J. **711**, 1033 (2010), 1001.0780.
[57] F. Schmidt, W. Hu, and M. Lima, Phys. Rev. D **81**, 063005 (2010), 0911.5178.
[58] J. Clampitt, B. Jain, and J. Khoury, ArXiv e-prints (2011), 1110.2177.
[59] Y. Li and W. Hu, ArXiv e-prints (2011), 1107.5120.